Nuclear Instruments and Methods in Physics Research A 681 (2012) 110–115

Contents lists available at SciVerse ScienceDirect

Nuclear Instruments and Methods in Physics Research A

journal homepage: www.elsevier.com/locate/nima

Measurement of neutron spectra generated by a 62 AMeV carbon-ion beam on a PMMA phantom using extended range Bonner sphere spectrometers

R. Bedogni [a,*], K. Amgarou [b], C. Domingo [b], S. Russo [c], G.A.P. Cirrone [c], M. Pelliccioni [a], A. Esposito [a], A. Pola [d], M.V. Introini [d], A. Gentile [a]

[a] Istituto Nazionale di Fisica Nucleare, Laboratori Nazionali di Frascati, Via E. Fermi 40, 00044 Frascati, Italy
[b] Grup de Recerca en Radiacions Ionitzants, Departament de Física, Universitat Autònoma de Barcelona, E-08193 Bellaterra, Spain
[c] Istituto Nazionale di Fisica Nucleare—Laboratori Nazionali dei Sud, Via S. Sofia 62, 95125 Catania, Italy
[d] Politecnico di Milano, CESNEF, Dipartimento di Energia, via Ponzio 34/3, 20133 Milano, Italy

ARTICLE INFO

Article history:
Received 20 March 2012
Received in revised form
5 April 2012
Accepted 5 April 2012
Available online 24 April 2012

Keywords:
Hadron therapy
Neutron spectrometry
Bonner sphere spectrometer
Unfolding
FRUIT

ABSTRACT

Neutrons constitute an important component of the radiation environment in hadron therapy accelerators. Their energy distribution may span from thermal up to hundred of MeV. The characterization of these fields in terms of dosimetric or spectrometric quantities is crucial for either the patient protection or the facility design aspects. To date, the Extended Range Bonner Sphere Spectrometer (ERBSS) is the only instrument able to simultaneously determine all spectral components in such workplaces. With the aim of providing useful data to the scientific community involved in neutron measurements at hadron therapy facilities, a measurement campaign was carried out at the Centro di AdroTerapia e Applicazioni Nucleari Avanzate (CATANA) of INFN-LNS (Laboratori Nazionali del Sud), where a 62 AMeV carbon ion is available. The beam was directed towards a PMMA phantom, simulating the patient, and two neutron measurement points were established at 0° and 90° with respect to the beam-line. The ERBSSs of UAB (Universidad Autónoma de Barcelona-Grup de Física de les Radiacions) and INFN (Istituto Nazionale di Fisica Nucleare-Laboratori Nazionali di Frascati) were used to measure the resulting neutron fields. The two ERBSSs use different detectors and sphere diameters, and have been independently calibrated. The FRUIT code was used to unfold the results.

1. Introduction

The carbon-ion therapy constitutes a significant fraction of the hadron therapy. According to the statistics of PTCOG (Particle Therapy Co-Operative Group, ptcog.web.psi.ch), it currently represents about 10% of the treatments performed in the about 30 existing hadron therapy facilities worldwide, and the variety of malignancies treatable with this technique is increasing [1].

The energy of interest for cancer therapy ranges from several tens up to 400 AMeV for carbon ions. Because the kinetic energy is significantly higher than the binding energy per nucleon (<8 MeV), the interaction of these ions with matter includes inelastic reactions with target and projectile fragmentation. A significant neutron production is always present. The neutron yield is roughly proportional to the energy per nucleon and weakly depends on the atomic number of the absorber. For carbon targets and 62 AMeV ions, the neutron yield is approximately 0.3 per incident ion [2].

Neutrons emitted at small angles mainly come from projectile-target peripheral collisions, where the incident ion may lose one or more nucleon. This has been modeled with the abrasion–ablation model [3]. The energy distribution has a maximum at approximately half the projectile initial energy per nucleon and extends up to about twice the projectile initial energy per nucleon.

At large angles, the neutron emission is mainly given by the evaporation processes occurring in the target and in the projectile. Therefore, the spectrum is softer and the fluence is lower than in the forward direction.

At therapeutic energies, neutrons constitute the main concern for either the occupational radiation protection and shielding, or the patient protection. Concerning the latter aspect, the neutron field produces a whole-body exposure of the patient, whilst the clinical beam selectively irradiates the treatment volume. As a consequence, the risk of long-term secondary cancer due to neutrons may be higher than that associated to the clinical beam and its scattered components [4,5].

Experimental works have been performed to quantify the neutron exposure in the vicinity of tissue equivalent phantoms irradiated with carbon-ion beams. Works using high-resolution

* Corresponding author. Tel.: +39 694032608; fax: +39 694032364.
E-mail address: roberto.bedogni@lnf.infn.it (R. Bedogni).

0168-9002/$ - see front matter © 2012 Elsevier B.V. All rights reserved.
http://dx.doi.org/10.1016/j.nima.2012.04.014

spectrometry techniques, like time-of-flight [6], normally focus on the high-energy component ($E > 20$ MeV). Works based on broad energy instruments like rem-meters [7,8] are also available in literature, but they cannot provide spectrometric information. In addition, the ambient dose equivalent ($H^*(10)$) response of rem-meters only partially matches the fluence-to-ambient dose equivalent conversion coefficient in limited energy ranges [9,10]. The mentioned works indicate that in-room neutron ambient dose equivalent largely depends on the beam delivery technique (active or passive scanning), on the projectile energy per nucleon, and on the materials composing collimators, energy degraders and other beam components. Reported $H^*(10)$ values span in the interval 0.05—few mSv per prescribed Gy at 1 m from the isocentre.

The aim of this work is to provide measured neutron spectra, covering all energies from thermal up to the maximum production energy, for the forward (0° with respect to the incident beam) and the sideward direction of a 62 AMeV carbon-ion beam impinging a PMMA target simulating the patient. In spite of its limited energy resolution, the Extended Range Bonner Sphere Spectrometers (ERBSS) [11] is the only spectrometer able to simultaneously determine all energy components from thermal up to the maximum expected energy ($\sim$100 MeV). Whilst a standard Bonner Sphere Spectrometer (BSS) [12] relies on polyethylene spheres and can generally measure up to 20 MeV neutrons, an ERBSS includes polyethylene spheres with high-Z (lead, copper, tungsten) inserts. At energy above 20 MeV, the inserts act as neutron multipliers and energy degraders through (n, xn) reactions. The response of the spectrometer is therefore extended in energy up to the GeV.

The experiment described in this work took place at the INFN-LNS (Istituto Nazionale di Fisica Nucleare-Laboratori Nazionali del Sud, Catania, Italy). The ERBSSs operated by the UAB and INFN groups were used to determine the neutron fluence spectra and the dosimetric quantities, namely the ambient dose equivalent $H^*(10)$.

The FRUIT code [13,14] was used to unfold the experimental data.

The UAB and INFN ERBSSs use different detectors, different set of spheres and have been independently calibrated. Comparison exercises [15,16] demonstrated the compatibility and the equivalence of these spectrometers. Particularly, they have been compared in the neutron field produced by a 62 MeV proton beam on a PMMA target [17]. Both spectrometers were used to determine the neutron spectra in the forward and sideward directions, obtaining coherent results (less than 5% difference in terms of total neutron fluence).

2. The UAB and INFN spectrometers

In the configuration used for this work, the INFN-ERBSS consisted of 7 polyethylene spheres, whose diameters are here labeled in inches units for convenience (2 in., 3 in., 5 in., 7 in., 8 in., 10 in., 12 in.), plus three extended range spheres with the following composition:

7(Pb): external diameter 7 in.; it includes an internal 4 in. polyethylene sphere surrounded by 1.27 cm of lead;
7(Cu): external diameter 7 in.; it includes an internal 4 in. polyethylene sphere surrounded by 1.27 cm of copper;
12(Pb):external diameter 12 in.; it includes an internal 3.15 in. polyethylene sphere surrounded by 1 cm of lead.

The UAB ERBSS relies on 8 polyethylene spheres (2.5 in., 3 in., 4.2 in., 5 in., 6 in., 8 in., 10 in. and 12 in.). A 1 mm thick cadmium (Cd) cover may be used in conjunction with the three smallest spheres and the resulting configurations are called 2.5(Cd), 3(Cd) and 4.2(Cd). The following extended range spheres are also included:

7(Pb): external diameter 7 in.; includes an internal 4 in. polyethylene sphere surrounded by 2.54 cm of lead;
7(Cu): external diameter 7 in.; includes an internal 4 in. polyethylene sphere surrounded by 2.54 cm of copper.

Details on the central detector, the response matrix and the calibration of the two spectrometers may be found in Refs. [15–21] for INFN system and in Refs. [15–17,22,23] for UAB system. For the purposes of this work it is worth recalling that the overall uncertainty of both response matrices was estimated as $\pm 3\%$ in the energy range below 20 MeV. As an example, the response matrix of the UAB ERBSS is reported in Fig. 1.

Because the neutron fields to be measured in this experience are expected to include large high-energy components ($E > 20$ MeV), a special consideration about extended range spheres and their uncertainty was done as follows.

Whilst the low-energy ($E < 20$ MeV) response of an ERBSS can be easily verified in monochromatic fields, no "pure" high-energy calibration fields are available in practice. Consequently, there is no direct way to estimate the uncertainty of the simulated high-energy response of the spheres. On the other hand, computational works have been carried out to assess the code-to-code variability in determining the high-energy response of extended range spheres [24]. In addition, simulation codes have been compared with experimental data on neutron production from targets at different energies and angles [25,26]. As a general conclusion, the code-to-code differences are limited to $\pm 10\%$ when estimating the ambient dose equivalent, the neutron fluence or the fluence in broad energy intervals. Following this indication, a $\pm 10\%$ uncertainty was assumed in this work for the high-energy response of the ERBSS. Because only the extended range spheres practically respond to high-energy neutrons, this uncertainty was only applied to the extended range spheres. The uncertainty of the response of standard polyethylene spheres, mainly responding to low-energy neutrons, was kept to $\pm 3\%$ as obtained in the validation experiments with mono-energetic neutron beams below 20 MeV.

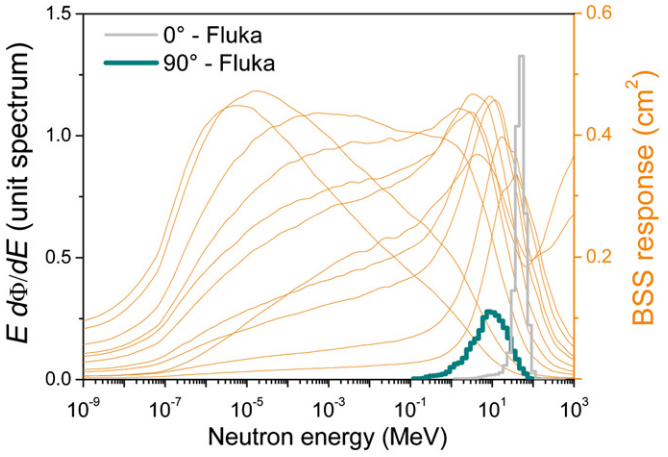

Fig. 1. Simulated neutron spectra in the forward (0°) and sideward (90°) directions superposed to the response functions of the UAB extended range Bonner Sphere spectrometer.

3. Unfolding

The unfolding problem in Bonner sphere spectrometry is under-determined, because the number of mathematical functions that could reproduce a given set of measured sphere counts is theoretically infinite. In principle, the spectrometric information increases as the number of spheres increases, but the amount of added information decreases for each added sphere, because the response functions are generally similar in shape and are partially superposed. This is also the reason why the energy resolution of the system is poor, especially in the energy regions where the response functions tend to be parallel [27]. This corresponds to the epithermal region and above 20 MeV. As a consequence, the pre-information plays a crucial role. Physically meaningful hypotheses must be formulated to supply the lack of information.

A variety of unfolding codes [28], providing pre-information in different ways, have been developed. In most cases they start from a default spectrum (or guess spectrum) that the user must provide. This is typically derived with Monte Carlo simulations. The unfolding code iteratively alters this spectrum attempting to reach a good agreement between the experimental counts and the "folded" counts, i.e. those obtained by folding the response matrix with the "candidate" spectrum. The FRUIT code embeds an option based on a special gradient algorithm [29]. This option is called FRUIT/SGM.

Alternatively, the knowledge of the physical processes at the basis of the neutron emission can be of great help. This is the "parametric" approach where the neutron spectrum is modeled as a superposition of elementary spectra covering the whole energy range and reflecting the neutron producing mechanisms. These elementary spectra are generated by the code and depend on a set of physically meaningful numerical parameters. The FRUIT [13] and NUBAY [30] codes include parametric unfolding options. They both perform statistical analyses to provide probability distributions for the parameters describing the neutron spectrum. Estimations of the parameter uncertainties can be done on these bases.

In its latest release (ver. six), FRUIT provides uncertainties of the neutron spectrum, which are specified bin per bin. The parametric option of FRUIT is convenient in a variety of operational scenarios, especially if detailed a priori information is not available. By contrast, when the final spectrum is likely to be obtained by slightly perturbing a highly reliable "default" spectrum, the FRUIT/SGM option may be used with accurate results.

Both parametric and SGM options of FRUIT have been used in the cited INFN—UAB comparison [17], providing very coherent results.

4. Monte Carlo simulations

A simplified Monte Carlo modeling of the irradiation scenario was performed to get a first estimation of the energy distribution of the ion-induced neutrons emerging from the PMMA phantom in the forward and sideward directions. These spectra also served as "default spectrum" for the FRUIT code, when operating in SGM mode.

A pencil $^{12}C^{6+}$ beam with energy 62 AMeV was supposed to impinge the $12\times12\times12$ cm^3 PMMA phantom (PMMA composition: $(C_5O_2H_8)_n$; density 1.2 g cm^{-3}). The whole system was considered in vacuum.

Simulations have been performed using the Monte Carlo transport code FLUKA version 2008.3b.1 [31,32]. FLUKA can transport more than 60 different particles plus heavy ions. Nuclear interactions generated by heavy ions were treated through interfaces to external event generators. The DPMJET code has been interfaced to cover the high (>5 GeV/n) energy range [33]. Between 0.125 and 5 GeV the interactions were treated by an extensively modified version of the RQMD-2.4 code (Relativistic Quantum Molecular Dynamics) [34–36]. At very low energy, below $\sim$0.1 GeV/n, a treatment based on the Boltzmann Master Equation (BME) has been implemented [37–39].

5. Irradiation set up

The measurements were carried out at the INFN-LNS superconducting cyclotron complex, in a room called "sala 0°". Fig. 2 shows a schematic diagram of the experimental arrangement used. The details on the carbon-ion beam line are given in Fig. 3. The PMMA phantom dimensions were $12\times12\times12$ cm^3.

The INFN ERBSS was exposed in point A whereas the UAB ERBSS was exposed in point B. The distances from the reference point in phantom were 110 cm in the forward direction and 190 cm in the sideward direction, respectively. The reference point was fixed at the Bragg peak position (approx. 7.6 mm in depth).

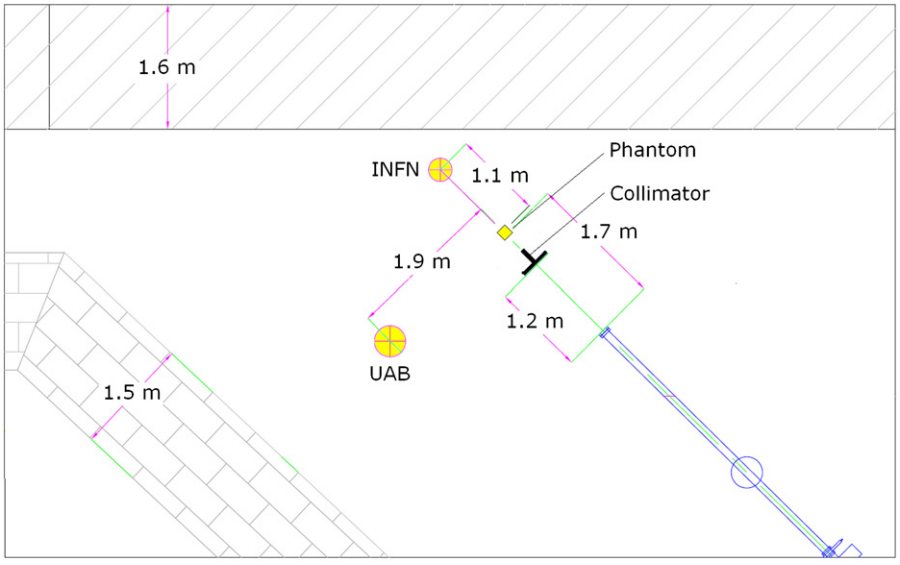

Fig. 2. View of the experimental room at INFN-LNS with indication of the measurement points. The locations where INFN and UAB systems were exposed are also identified as points A and B, respectively.

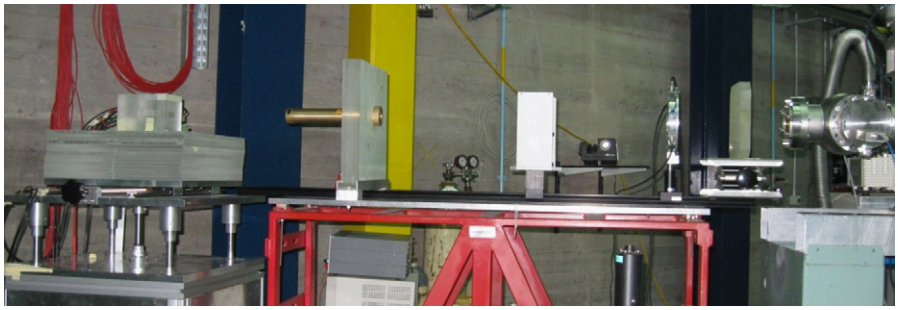

Fig. 3. Carbon-ion beam line. From the right: beam exit, PMMA collimator, monitor ion chamber, beam-centering system, final collimator and PMMA phantom.

The Bonner spheres were sequentially exposed, choosing irradiation times sufficient to achieve statistical counting uncertainties lower than $\pm 1\%$.

Because the carbon ion current varied significantly during the irradiation (in the order of $\pm 10\%$), the following normalization procedure was adopted. Two neutron sensitive monitor instruments were installed in the irradiation room, namely a Thermo FHT 62 rem-counter and a 4.2 in. polyethylene sphere with a cylindrical (10 mm diameter and 9 mm high) ^{3}He filled (8 kPa) thermal neutron counter. These instruments were placed in the vicinity of the two ERBSS and were continuously acquiring during the whole irradiation period. For normalization purposes, these instruments and a reference ion chamber calibrated in terms of absorbed dose in tissue at the conventional depth of 3 mm, were simultaneously exposed. The coherence between the two neutron sensitive monitors was checked by measuring their ratio in different time intervals. The variation of this ratio was always lower than $\pm 3\%$ (one s.d.). This was regarded as monitoring uncertainty.

For each ERBSS, the experimental counts were divided by the reading of the respective monitor instrument. The result, called normalized ERBSS counts, was used as input data for the unfolding procedures. The uncertainties of the normalized ERBSS counts, obtained by a quadratic combination of counting uncertainties (between $\pm 0.5\%$ and $\pm 1\%$) and of the monitoring uncertainty ($\pm 3\%$), were always lower than 4%.

6. Results and discussion

6.1. Simulations

Fig. 1 gives lethargy plots of the simulated neutron spectra in points A (0°) and B (90°), normalized to the total fluence (unit spectrum) and in equi-lethargy representation. To understand how the response of an ERBSS and these spectra are matching in terms of energy interval, these plots are superposed to the response functions of the UAB ERBSS. Because the simulation does not include the air, the walls and the other materials present in the room, these spectra do not include neutrons below 0.1 MeV.

The simulated spectrum in the forward direction presents the maximum fluence at approximately half the ion energy per nucleon (approx. 30 MeV). Because the plot is equi-lethargic, the maximum appears at a higher value (between 50 and 60 MeV). Neutron energies extend up to more than 100 MeV. The sideward spectrum is considerably broader and softer.

6.2. Measurements

The neutron spectra in the 0° and 90° directions were obtained by unfolding the ERBSS data with the FRUIT code, used in both parametric or SGM mode.

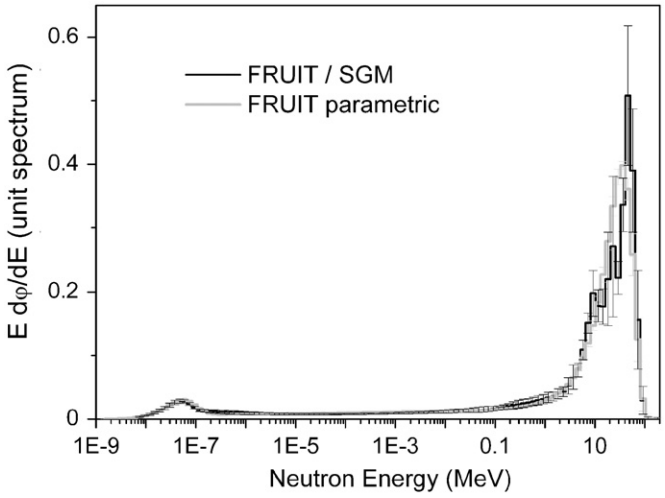

Fig. 4. Unfolded neutron spectrum in the forward direction.

The following data were introduced in the unfolding code: the normalized ERBSS counts, their uncertainties ($< \pm 4\%$, one s.d.), the ERBSS response matrix and its uncertainty ($\pm 3\%$ for the standard polyethylene spheres and $\pm 10\%$ for the extended range spheres, as explained in Section 2).

For unfolding in SGM mode, default spectra were assembled by adding a thermal component (5% of the total fluence) and an epithermal $1/E$ continuous (5% of the total fluence) to the FLUKA spectra. Repeated tests showed that the results of the unfolding were not affected by the amount of thermal and epithermal neutrons included in the default spectra, neither by the shape of the epithermal continuous.

The unfolded spectra are shown in Figs. 4 and 5. In all cases the energy distribution is coherent with the FLUKA predictions, taking into account the limited energy resolution of the system. A good agreement exists between the parametric and SGM solutions for both INFN and UAB spectrometers.

Uncertainty bars specified on a bin-per-bin basis can be used to roughly compare the resolving power of the spectrometer in different energy intervals. These are in the order of $<20\%$ in the eV region; 10–20% from 1 eV to 10 keV; 20–25% from 10 keV to 1 MeV; $\sim$20% from 1 to 10 MeV; $\sim$30% above 10 MeV. These uncertainties come from the propagation of the input data uncertainties σ_{in}, which is a quadratic combination of the uncertainties on the normalized BSS and on the response functions, through the unfolding procedure. This propagation is done by randomly generating a large number ($>10^3$) of sets of BSS counts, using σ_{in} as amplitude of the Gaussian perturbation, and then separately unfolding each set. The uncertainties of the spectrum and of any spectrum-related quantity are

obtained from the statistical distribution of the results of this propagation.

The spectrum integrated quantities such as the H*(10) value, the spectrum-average fluence-to-H*(10) conversion coefficient, h*(10), and the total fluence, are provided in Table 1. Also the fractions of fluence under specific energy intervals are reported in this table, namely the thermal domain ($E < 0.5$ eV), the epithermal domain ($0.5\ \text{eV} < E < 10\ \text{keV}$), the fast neutron domain ($10\ \text{keV} < E < 1\ \text{MeV}$) and the high-energy domain ($E > 1$ MeV), which corresponds to the main peak.

Because of the complexity of the unfolding process, one may point out that it is difficult to know whether the final spectra are coherent with the real experimental data (the normalized ERBSS counts). This is shown in Figs. 6 and 7. Here the normalized ERBSS counts are compared with the "folded" counts, i.e. those obtained by folding the ERBSS response matrix with the unfolded spectra. Uncertainty bars are the quadratic combination of uncertainties of the normalized BSS counts (less than $\pm 4\%$) with the overall uncertainties of the response functions ($\pm 3\%$ for the standard polyethylene spheres and $\pm 10\%$ for the extended range spheres). The folded counts are always in agreement with the experimental counts, thus confirming the coherence between the unfolded spectra and the experimental data.

6.3. Comparing the forward and the sideward directions

From Fig. 8 and Table 1 it is evident the different energy composition of the neutron fields in the forward and sideward directions. An additional comment is needed to explain why the total fluence at 0° has higher uncertainty ($\pm 7\%$) than that at 90° ($\pm 3\%$). This is because the high-energy component at 0° is considerably larger than at 90°, and the response function of the extended range spheres, used to estimate this component, have

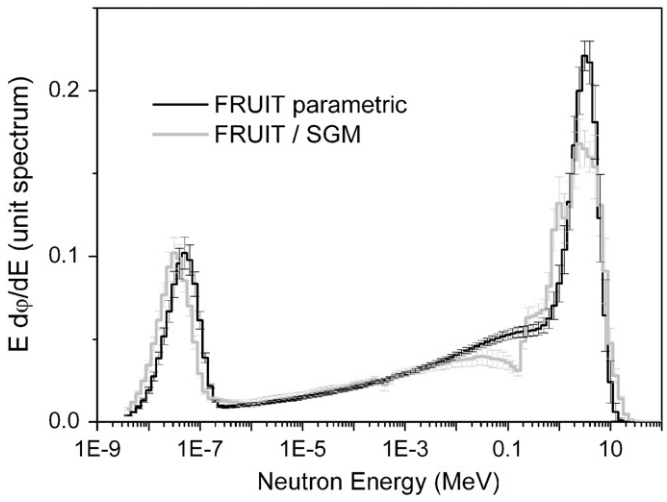

Fig. 5. Unfolded neutron spectrum in the sideward direction.

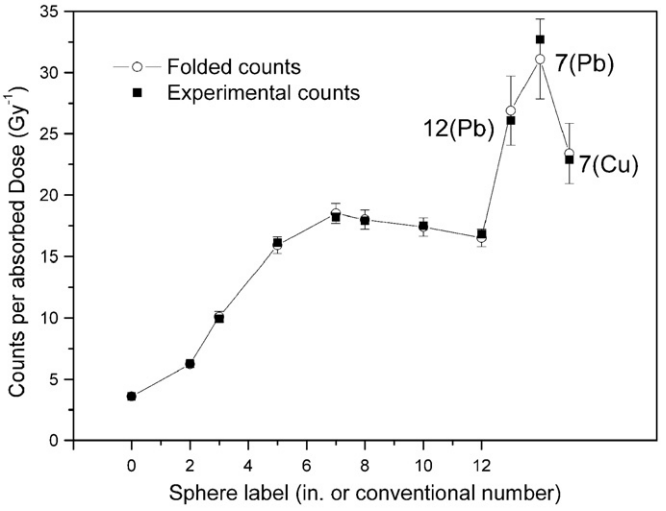

Fig. 6. Measurements in the forward direction. The experimental counts are compared with the "folded" counts, obtained by folding the ERBSS response matrix with the unfolded spectrum. Uncertainty bars are the quadratic combination of uncertainties of the normalized BSS counts (less than $\pm 4\%$) with the overall uncertainties of the response functions ($\pm 3\%$ for the standard polyethylene spheres and $\pm 10\%$ for the extended range spheres). For the standard polyethylene spheres, the diameter in units of in. is given by the X axis.

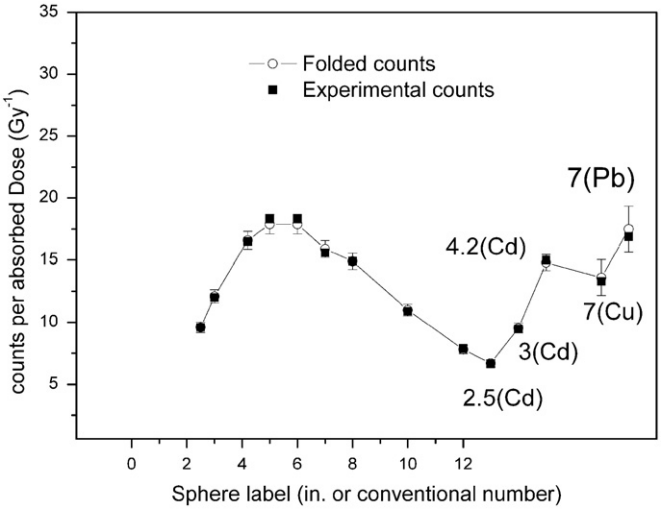

Fig. 7. Measurements in the sideward direction. The experimental counts are compared with the "folded" counts, obtained by folding the ERBSS response matrix with the unfolded spectrum. Uncertainty bars are the quadratic combination of uncertainties of the normalized BSS counts (less than $\pm 4\%$) with the overall uncertainties of the response functions ($\pm 3\%$ for the standard polyethylene spheres and $\pm 10\%$ for the extended range spheres). For the standard polyethylene spheres, the diameter in units of in. is given by the X axis.

Table 1
Spectrum integrated quantities for the spectra measured in the forward and sideward directions.

Direction	Unfolding method	Point	$h^*(10)$ (pSv cm^2)	Fluence (cm^{-2} Gy^{-1})	$H^*(10)$ (nSv Gy^{-1})	Fluence fractions			
						$E < 0.5$ eV	0.5 eV–10 keV	10 keV–1 MeV	$E > 1$ MeV
0°	Parametric	A	371 ± 7	276 ± 10	102 ± 5	6.7%	8.5%	8.9%	75.9%
	SGM	A	376 ± 7	279 ± 19	105 ± 7	6.8%	7.5%	10.6%	75.1%
90°	Parametric	B	185 ± 4	65 ± 2	12.0 ± 0.4	20.0%	20.9%	23.9%	35.2%
	SGM	B	184 ± 5	66 ± 2	12.2 ± 0.4	21.3%	21.5%	22.6%	34.6%

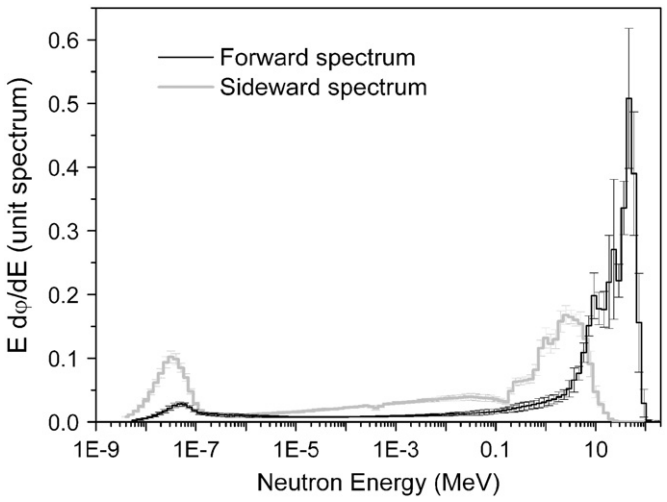

Fig. 8. Comparison between the neutron spectra measured in the forward and in the sideward directions.

larger uncertainty than the standard polyethylene spheres. This reflects in

1) an increase in the spectrum uncertainty bars as the neutron energy increases above 10 MeV;
2) an increased uncertainty in the total fluence when moving from 90° to 0°.

It should be also noted that at 0° (see Fig. 6) the extended range spheres count a factor of two more than the standard spheres, whilst they count nearly the same at 90° (See Fig. 7). This also indicates the very different energy distribution of the neutron fields in the two directions.

If the H*(10) values are reported to the conventional distance of 1 m from the target, the results are in the order of 0.1 mSv/Gy at 0° and 0.04 mSv/Gy at 90° (inverse square distance correction was applied as a first approximation).

7. Conclusions

The neutron fields generated in the forward and sideward directions from a PMMA phantom bombarded with 62 AMeV carbon ions were determined using two independent extended range Bonner Sphere spectrometers.

The FRUIT unfolding code was used in both SGM mode (requiring a default spectrum) and parametric mode (not requiring default spectrum, but using built-in elementary spectra). The final spectra basically do not depend on the unfolding mode and the spectrum-integrated quantities are fully compatible.

The quality of the spectrum in the forward and sideward direction is very different, as expected from the FLUKA simulations. Particularly, the forward spectrum exhibits a sharp peak at approx. 50 MeV. In spite of the known poor energy resolution, the ERBSS allowed to correctly identify the main structures present in the neutron spectra and to provide precise estimations for the spectrum-integrated quantities like the fluence and the ambient dose equivalent.

Taking into account that the recent literature offers a limited number of measured neutron spectra at hadron-therapy facilities, the results of this work may be of help for both medical physicist and radiation protection communities.

Acknowledgments

This work was supported by the Spanish Ministerio de Ciencia e Innovación (MICINN) under contract FIS2006-01843, by the INFN-MEC/MICINN bilateral agreement and by the INFN projects MicroSi and NESCOFI@BTF (Commissione Scientifica Nazionale CSN 5).

References

[1] A.D. Jensen, A.V. Nikoghosyan, S. Ecker, M. Ellerbrock, J. Debus, M.W. Münter, Radiation Oncology 6 (2011) 30.
[2] F. Clapier, C.S. Zaidins, Nuclear Instruments and Methods A 217 (1983) 489.
[3] R. Serber, Physical Review 72 (1947) 1114.
[4] W.D. Newhauser, J.D. Fontenot, A. Mahajan, D. Kornguth, M. Stovall, Y. Zheng, P.J. Taddei, D. Mirkovic, R. Mohan, J.D. Cox, S. Woo, Physics in Medicine and Biology 54 (8) (2009) 2277.
[5] H. Nystrom, D.I. Thwaites, Radiotherapy and Oncology 86 (2008) 1.
[6] K. Gunzert-Marx, H. Iwase, D. Schardt, R.S. Simon, New Journal of Physics 10 (2008) 075003.
[7] S. Yonai, N. Matsufuji, T. Kanai, Y. Matsui, K. Matsushita, H. Yamashita, M. Numano, T. Sakae, T. Terunuma, T. Nishio, R. Kohno, T. Akagi, Medical Physics 35 (11) (2008) 4782.
[8] S. You Wu, L. Zong-Qiang, L. Wu-Yuan, W. Gui-Ling, Chinese Physics C 34 (5) (2010) 548.
[9] International Commission on Radiological Protrection (ICRP), Conversion coefficients for use in radiological protection against external radiation, ICRP publication 74, Ann. ICRP 26, Pergamon Press, 1996.
[10] M. Pelliccioni, Radiation Protection Dosimetry 88 (2000) 279.
[11] B. Wiegel, A.V. Alevra, Nuclear Instruments and Methods A 476 (2002) 36.
[12] A.V. Alevra, D.J. Thomas, Radiation Protection Dosimetry 107 (1–3) (2003) 37.
[13] R. Bedogni, C. Domingo, A. Esposito, F. Fernández, Nuclear Instruments and Methods A 580 (2007) 1301.
[14] R. Bedogni, M. Pelliccioni, A. Esposito, Nuclear Instruments and Methods A 615 (2010) 78.
[15] R. Bedogni, C. Domingo, A. Esposito, M. Chiti, M.J. García-Fusté, G. Lovestam, Nuclear Instruments and Methods A 620 (2010) 391.
[16] A. Esposito, R. Bedogni, C. Domingo, M.J. García, K. Amgarou, Radiation Measurements 45 (2010) 1522.
[17] K. Amgarou, R. Bedogni, C. Domingo, A. Esposito, A. Gentile, G. Carinci, S. Russo, Nuclear Instruments and Methods A 654 (2011) 399.
[18] R. Bedogni, A. Esposito, Nuclear Technology 168 (2009) 615.
[19] R. Bedogni, Ph.D. Thesis, Universidad Autonoma de Barcelona, Barcelona, Spain, 2006.
[20] R. Bedogni, A. Esposito, A. Gentile, M. Angelone, M. Pillon, Radiation Measurements 46 (2011) 1757.
[21] B. Wiegel, et al., Radiation Measurements 44 (7–8) (2009) 660.
[22] M. Bakali, Ph.D. Thesis, Universidad Autonoma de Barcelona, Barcelona, Spain, (2001) (in Spanish).
[23] V. Lacoste, V. Gressier, J.-L. Pochat, F. Fernandez, M. Bakali, T. Bouassoule, Radiation Protection Dosimetry 110 (2004) 529.
[24] C. Pioch, V. Mares, W. Ruhm, Radiation Measurements 45 (2010) 1263.
[25] Van der Meer, et al., Nuclear Instruments and Methods B 217 (2004) 202.
[26] B. Rapp, J.-C. David, V. Blideanu, D. Doré, D. Ridikas, N. Thiollière, Benchmarking of the Modelling Tools Within the EURISOL DS project, Proceedings of the Eighth Specialists Meeting on Shielding Aspects of Accelerators, Targets and Irradiation Facilities (SATIF-8), Pohang, South Korea, 22–24 May 2006, OECD Nuclear Energy Agency, 2010, pp. 251–260.
[27] M. Reginatto, Nuclear Instruments and Methods A 480 (2–3) (2002) 690.
[28] M. Matzke, Radiation Protection Dosimetry 107 (1–3) (2003) 155.
[29] M. Matzke, Unfolding of Pulse Height Spectra: The HEPRO Program System, Report PTB-N 19, Braunschweig: Physikalisch-Technische Bundesanstalt, 1994.
[30] M. Reginatto, Radiation Protection Dosimetry 121 (2006) 64.
[31] A. Fassò, A. Ferrari, J. Ranft, P.R. Sala, FLUKA: A Multi-Particle Transport Code, CERN-2005-10, 2005, INFN/TC_05/11, SLAC-R-773.
[32] G. Battistoni, S. Muraro, P.R. Sala, F. Cerutti, A. Ferrari, S. Roesler, A. Fassò, J. Ranft, The FLUKA Code: Description and Benchmarking, Proceedings of the Hadronic Shower Simulation Workshop 2006, Fermilab 6–8 September 2006, M. Albrow, R. Raja eds., AIP Conference Proceeding 896, 2007, pp. 31–49.
[33] S. Roesler, R. Engel, J. Ranft, The Monte Carlo Event Generator DPMJET-III, in: Proceedings of the Monte Carlo 2000 Conference, Lisbon, October 23–26 2000, A. Kling, F. Barao, M. Nakagawa, L. Tavora, P. Vaz eds., Springer-Verlag, Berlin, 2001, pp. 1033–1038.
[34] H. Sorge, H. Stoecker, W. Greine, Annals of Physics 192 (1989) 266.
[35] H. Sorge, H. Stoecker, W. Greiner, Nuclear Physics A498 (1989) 567.
[36] H. Sorge, Physical Review C52 (1995) 3291.
[37] M. Cavinato, E. Fabrici, E. Gadioli, E. Gadioli Erba, E. Galbiati, Physics Letters B382 (1996) 1.
[38] M. Cavinato, E. Fabrici, E. Gadioli, E. Gadioli Erba, G. Riva, Nuclear Physics A679 (2001) 753.
[39] F. Cerutti, G. Battistoni, G. Capezzali, P. Colleoni, A. Ferrari, E. Gadioli, A. Mairani, A. Pepe, Low Energy Nucleus–Nucleus Reactions: The BME Approach and its Interface with FLUKA, in: Proceedings of the 11th International Conference on Nuclear Reaction Mechanisms, Varenna (Italy), June 12–16, 2006.